

# Learning Friction Model for Magnet-actuated Tethered Capsule Robot

Yi Wang<sup>1,a</sup>, Yuyang Tu<sup>2,a</sup>, Yuchen He<sup>3</sup>, Xutian Deng<sup>1</sup>, Ziwei Lei<sup>1</sup>, Jianwei Zhang<sup>2</sup> and Miao Li<sup>†1</sup>

**Abstract**—With the potential applications of capsule robots in medical endoscopy, accurate dynamic control of the capsule robot is becoming more and more important. In the scale of a capsule robot, the friction between the capsule and the environment plays an essential role in the dynamic model, which is usually challenging to model beforehand. In the paper, a tethered capsule robot system driven by a robot manipulator is built, with a strong magnetic Halbach array mounted on the robot’s end-effector to actuate the capsule. The friction between the capsule and the environment is learned with demonstrated trajectories to increase the control accuracy. Experimental results shown an improvement of 5.6% in terms of tracking error and the stability of the contact force is improved by about 6.2%.

**Keywords**— tethered capsule robot, magnetic actuation, friction model

## I. INTRODUCTION

Capsule endoscopy robots are commonly used for clinical intestinal and stomach inspections. The capsule robot enters the body by being swallowed or being placed into the patient’s intestines. Capsule robots divided into two distinct types: tethered [1] and wireless [2]. The tethered capsule robot has obvious advantages of scalability and repeatability compared with wireless. The tether can provide a stable video transmission channel and enough light, which can efficiently support the inspection and treatment of the digestive tract, stomach and other parts [3]. To achieve various functions based on the premise that the robot is to be pulled to target-point. The most effective control scheme is the external magnetic-field driver [4]. The external magnetic-field can be provided in three methods: the permanent magnet-combined current coil [5], the permanent magnet [6], and a three-axis Helmholtz magnetic coil [7].

The external magnetic-field driver can effectively overcome the problem that the tethered capsule cannot move passively through peristalsis of the digestive tract. A driving method of hand-held permanent magnet device is proposed in [8], the method mount the motor on the permanent magnet to solve the problem of multi-degree-of-freedom operation.

<sup>1</sup> School of Power and Mechanical Engineering, Wuhan University, Hubei, China (e-mail: miao.li@whu.edu.cn)

<sup>2</sup> Department of Informatics, University of Hamburg, School of Mechanical Engineering and Automation (e-mail: yuyang.tu@studium.uni-hamburg.de)

<sup>3</sup> School of Mechanical Engineering and Automation, Wuhan Textile University, Hubei (e-mail: heyuchen2021@outlook.com)

<sup>a</sup> These authors have contributed equally to this work.

<sup>†</sup> Corresponding author.

This work was supported by the Natural Science Foundation of Jiangsu Province (Grant No. BK20180235) and the German Research Foundation (DFG) and the National Science Foundation of China in project Crossmodal Learning, TRR-169.

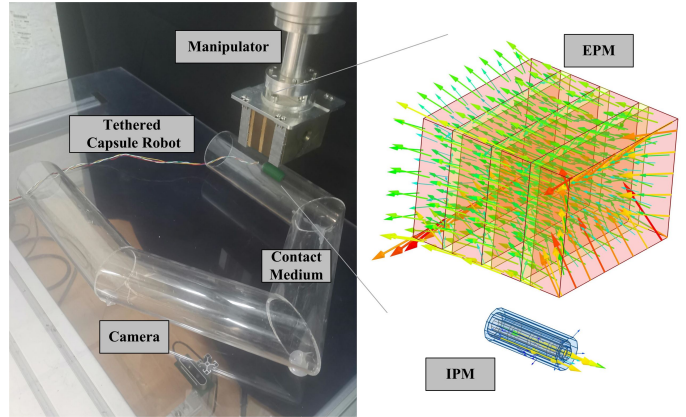


Fig. 1. The picture shows the overall scene and magnetic-field of the magnet: At the end of the manipulator is a external permanent magnet (EPM), and an inner permanent magnet (IPM) is inside the tethered capsule robot. Contact medium is an obstacle between IPM and EPM.

To further explore this problem, a new control algorithms based on the manipulator and three-axis transplanting table are proposed in [1] and [5]. However, the key problem of driving control is modeling the tethered. There are some unknown factors in the model of the tethered capsule robot, which generally come from the friction between the tethered and the environment.

In order to analyze the friction factor between the capsule and the environment, the speed of the capsule robot and the resistance model of the intestine were established [9], and the design parameters of the robot capsule endoscope were used in the resistance model [4]. But, these methods cannot obtained the accurate friction force, so Kim *et al.* made a specially designed tribological tester to study the influence of capsule shape on frictional resistance characteristics [10]. A constant velocity friction model was established to study the influence of contact deformation on friction [11]. Despite these model-methods have some effects, but these methods do not quantitatively analyze the friction and drag caused by the tethered.

This paper proposes a dynamic model with friction to compensate the movement of the tethered capsule robot. First, we analyzed all force of the tethered capsule robot, including gravity, contact force with mediums, and the tractive-force and friction by the tethered. Second, movement data of friction model can be collected from the plane motion

between the tethered capsule robot and contact mediums. Furthermore, we obtained the specific friction model of the tethered capsule robot by learning the data. Finally, model-constraints were added between the preset trajectory point velocities of the control algorithm to keep the velocity within the velocity range of the friction model, which could reduce the trajectory error of the capsule movement and the fluctuation of the contact force.

The main contribution of our research is to give a learning friction model, which has the potential to apply the motion control to the tethered capsule robot in mediums with any friction coefficient. In addition, the article provides a plane experiment method to obtain friction model of the tethered capsule robot, and further guides the capsule movement control. The organizational structure of this paper is as follows: In Section II, the theory of capsule friction model is proposed. In Section III, the entire experimental system, magnetic-field simulation method and the process of obtaining the friction model are introduced. In Section IV, the validity of the friction theory in the current experimental environment is verified through experiments. In Section V, the whole research work and results of this article are summarized.

## II. PROBLEM STATEMENT

The key to control the tethered capsule is the modeling of the tethered capsule system. Fig. 2 shows the force diagram of the tethered capsule during movement. A friction dynamic model between the capsule robot and the contact interface is proposed to optimize the motion control of the capsule robot attached to different mediums [11], [12], [13]. We expect to obtain a more specific friction relationship between the capsule robot and the environment to improve the control accuracy.

### A. Dynamic Model of Magnetron Capsule

According to the application of the point dipole model in [7], [11], the theoretical dynamic model of magnetron capsule is defined as:

$$B(x)\ddot{x} + C(x, \dot{x})\dot{x} + G(x) = \tau_m(x, q) \quad (1)$$

where  $x \in \mathbb{R}^3$  is the capsule pose (position and orientation) and  $q \in \mathbb{R}^6$  embeds the robot joint variables; matrices  $B(x)$ ,  $C(x, \dot{x})$ ,  $G(x)$  are the inertia, Coriolis matrix and gravity of the capsule respectively. The vector  $\tau_m(x, q) \in \mathbb{R}^6$  represents the magnetic force and torque exerted by the EPM on the IPM, which is highly non-linear. Our aim is to find  $q$  such that  $x$  approaches a desired value  $x_d$ .

In order to get a controllable position control scheme, the differential of (1) can be deduced as the following expression:

$$\dot{\tau}_m = \frac{\partial \tau(x, q)}{\partial x} \dot{x} + \frac{\partial \tau(x, q)}{\partial q} \dot{q} = J_x \dot{x} + J_q \dot{q} \quad (2)$$

$J_x$  and  $J_q$  are derived in the [11],  $\tau_m$  is the state variable of the control system [11]. Other parameters are shown in Table I. The dynamic model with friction compensation of

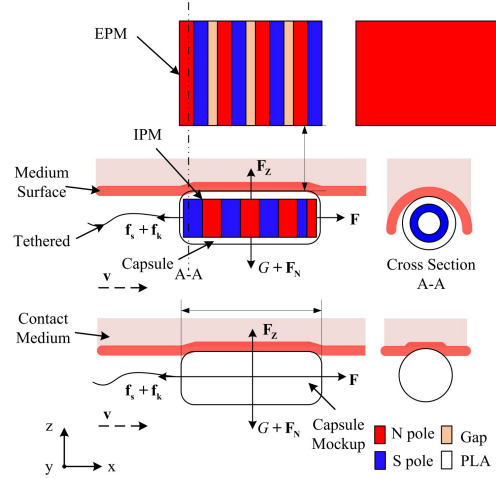


Fig. 2. The force diagram of the magnetron capsule.

the magnetron capsule can be expanded to (3) by combining (1) and (2):

$$\begin{cases} B(x)\ddot{x} + C(x, \dot{x})\dot{x} + G(x) = \tau_m(x, q) \\ \dot{\tau}_m(x, q) = J_x \dot{x} + J_q \dot{q} + \dot{\kappa} \end{cases} \quad (3)$$

### B. Friction Model Establishment

The  $\dot{\kappa}$  mentioned in (3) is put as equivalent to a straight connecting rod in the simulation environment [11], which is not verified in the current research. In the real environment,  $\dot{\kappa}$  is judged to represent the friction between the capsule and the environment, including kinetic friction force  $f_k$  and static friction force  $f_s$ . The theoretical kinetic model of magnetron capsules can be expressed as (Other parameters are shown in Table I):

$$\mathbf{F} + \mathbf{f}_s + \mathbf{f}_k = m\mathbf{a}, \mathbf{f}_k = \mathbf{F}_N \cdot \mu \quad (4)$$

$$\mathbf{F} + \mathbf{f}_s + \mathbf{F}_N \cdot \mu = m\mathbf{a}$$

In particular, kinetic friction and static friction have been proved to be relative. These two concepts can be replaced by a view of rate-dependent friction, the law of friction of rocks [13], which is generally applicable to materials including polymers, glasses, etc. In [13], the coefficient of friction is related to instantaneous velocity  $\mathbf{v}$  and state variable  $\theta$ .

$$\mu = \mu_0 - a \ln \left( \frac{|\mathbf{v}^*|}{|\mathbf{v}|} + 1 \right) + b \ln \left( \frac{\mathbf{v}^* \theta}{D_c} + 1 \right) \quad (5)$$

$|\mathbf{v}| \ll \mathbf{v}^*$ , the expression of friction law (5) can be rewritten as:

$$\mu = \mu_0 - (a - b) \ln \left( \frac{|\mathbf{v}^*|}{|\mathbf{v}|} + 1 \right) \quad (6)$$

We assume  $c$  is the relationship  $(a - b)$  that is a friction factor of the friction model, so the friction model can be predicted by substituting (6) into (4):

$$\mathbf{F} + \mathbf{f}_s + \mathbf{F}_N \cdot \left[ \mu_0 - c \cdot \ln \left( \frac{\mathbf{v}^*}{|\mathbf{v}|} + 1 \right) \right] = m\mathbf{a} \quad (7)$$

TABLE I  
NOMENCLATURE USED

Symbol	Description
$\kappa$	All friction between capsule and Environment
$\mathbf{F}$	Traction Force of capsule in Movement Direction
$\mathbf{F}_z$	Magnetic Force of capsule in Vertical Direction
$\mathbf{F}_N$	Supporting Force of capsule in Vertical Direction
$\mathbf{f}_s$	Static Friction Force
$\mathbf{f}_k$	Kinetic Friction Force
$m$	Capsule Mass (20.9g)
$\mathbf{a}$	Capsule Acceleration
$\mathbf{v}$	Manipulator Speed (Preset Experimental Speed)
$\mathbf{v}^*$	The Typical Speed, about 0.2m/s [12]
$D_c$	Critical Slip Length [12]
$a$	System Constant [12],[13]
$b$	System Constant [12],[13]
$\mu_0$	Sliding Friction Coefficient
$c$	Equation of Friction System to be Solved.

### III. EXPERIMENTAL

#### A. Experimental System Setup

As shown in Fig. (3), the overall hardware system mainly consists of EPM, IPM and manipulator. At present, permanent magnet is the one of most commonly used approach to provide stable and strong magnetic-field, which shapes mainly including cylinder [5], ring [6] and cube [14]. The EPM terminal designed in this paper is composed of four strong cubic magnets in a Halbach Array [15] which can be applied to increase magnetic field range and strength shown in Fig. (3)(b). EPM is connected to the manipulator through 6061 aluminum alloy to avoid the influence of strong magnetism. As shown in Fig. 3(c), the IPM design is largely inspired by the work in [16], and in our case a tethered robot is used. The weight, length, and diameter of the capsule robot are 20.9g, 36mm, and 14mm respectively. The detailed structure of the tethered capsule robot is shown in Fig. 3(c). During the movement, the capsule robot is attached to the PVC plate by the external magnetic force. A transparent PVC plate is supposed to facilitate camera calibration and collect the motion information of the capsule robot.

As shown in (7), the friction model established in this paper can be applied to mediums with different sliding friction coefficients. According to the friction coefficient between PVC and PLA [17], [18], and the test tension range of the relative movement of PLA and PVC is 0.042~0.048N, we set the sliding friction coefficient of PVC transparent

plate and capsule robot as 0.22. After same process are repeated on paper and polyester-cloth, we get that the friction coefficient of the robot on paper is 0.26 [19], and the friction coefficient on polyester-cloth is 0.19 [20].

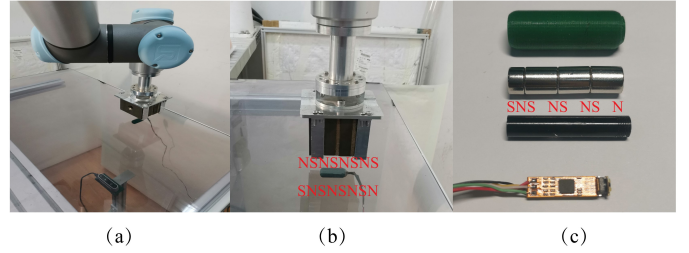


Fig. 3. Structure of system: (a) Schematic diagram of the overall scene. (b) Working diagram of EPM and IPM. (c) A detail drawing of the capsule robot.

#### B. Acquire $\mathbf{F}$ and $\mathbf{F}_z$ in Friction Model

The drag force  $\mathbf{f}_s$  of the system is measured using the tension dynamometer, which is 0.03N.  $\mathbf{F}$  and  $\mathbf{F}_z$  are obtained by theoretical simulation (Fig. (4)). From (7), the ambient friction force of the capsule robot can be compensated by adjusting the  $\mathbf{v}$  of the manipulator, to determine the force of the capsule robot. In the way, the instantaneous acceleration of the capsule robot can be controlled, but this friction relation  $c$  must be determined in advance, the detailed acquisition steps are as follows.

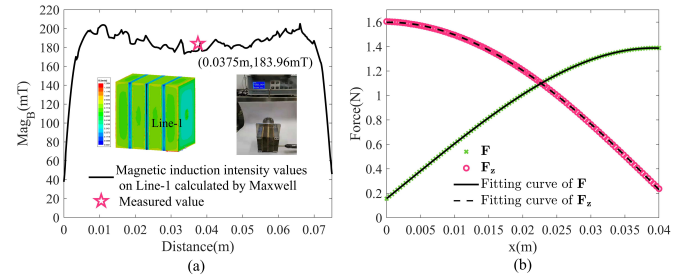


Fig. 4. Results of finite element analysis: (a) Comparison of simulated and measured values. (b) Simulation value and fitting curve of  $\mathbf{F}$  and  $\mathbf{F}_z$ .

The steps for Maxwell to acquire  $\mathbf{F}$  and  $\mathbf{F}_z$  are as follows: First, the field source IPM and EPM are processed by the equivalent volume current method. Then the magnetic-field distribution is obtained according to the homogeneous wave equations. Finally, the electromagnetic force [21] on the IPM is calculated based on the principle of virtual work, which can be given by:

$$\mathbf{F} = \frac{dW}{ds} = \frac{\partial}{\partial \mathbf{s}} \left[ \int_V \left( \int_0^H \mathbf{B} \cdot d\mathbf{H} \right) dV \right] \quad (8)$$

where  $ds$  is virtual displacement,  $W$  is the total magnetic field energy of the system,  $V$  is the volume of the IPM,  $\mathbf{B}$  is the magnetic flux density, and  $\mathbf{H}$  is the magnetic-field strength.

To verify the validity of the simulation parameters settings (see Table II). We compared the value of magnetic induction measured by maxwell and Gauss meter on Line-1 of the field source EPM (see Fig 4(a)). The relative error between the simulation results and the measured data is 4.11% (more comparison results see Supplementary Video). The values of  $\mathbf{F}$  and  $\mathbf{F}_z$  (see Fig 4(b)) on the IPM are calculated by the three-dimensional transient solver when the EPM moves in the x-direction at a constant speed of 0.01m/s. With the force trend of the simulation calculation results, the relationship between the electromagnetic force and the relative distance is obtained by polynomial fitting [22] (see Fig 4(b)). The root mean squared errors (RMSE) fitted by  $\mathbf{F}$  and  $\mathbf{F}_z$  are 0.068% and 0.294%, respectively.

TABLE II  
PARAMETERS OF EPM AND IPM

Parameter	EPM	IPM
Effective Length (mm)	60	35
Effective Width / Outer Diameter (mm)	75	D10
Effective Height / Internal Diameter (mm)	55	D6
Material	NdFe30	NdFe30

### C. Acquire $\mathbf{v}$ and $\mathbf{a}$ in Friction Model

The coordinates of the end of the manipulator and the capsule robot are read at the same frequency (20Hz). Fig. 5(a)-(d) shows the capsule trajectory tracking process. The velocities  $\mathbf{v}$  of EPM and IPM can be calculated by  $\frac{\Delta(\mathbf{P}_x - \mathbf{P}_{x-1})}{\Delta t}$  after each point in the trajectory recorded into system.  $\chi$  indicates the point in time. The coordinate data of the EPM ( $\mathbf{P}_E \in \mathbb{R}^3$ ) at the end of the robotic arm are directly read from the ROS node. The tethered capsule robot acceleration  $\mathbf{a}$  can be obtained by calculating  $\frac{\Delta(\mathbf{V}_x - \mathbf{V}_{x-1})}{\Delta t}$ , where ( $\mathbf{P}_I \in \mathbb{R}^3$ ) is the coordinate information of the capsule robot collected by the camera. The friction model of the tethered capsule can be analyze more scientifically by collecting movement data in four directions: up, down, left, and right. The data points above in each movement interval at 10s intervals to reduce random errors. Detail is shown in Fig. 6.

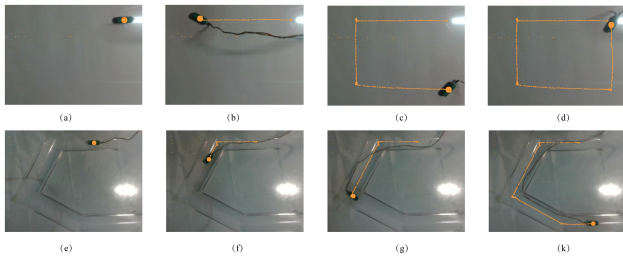


Fig. 5. The trajectory tracking process of the capsule robot: (a)-(d) The rectangular trajectory of the capsule robot. (e)-(k) Bend pipe trajectory of the capsule robot.

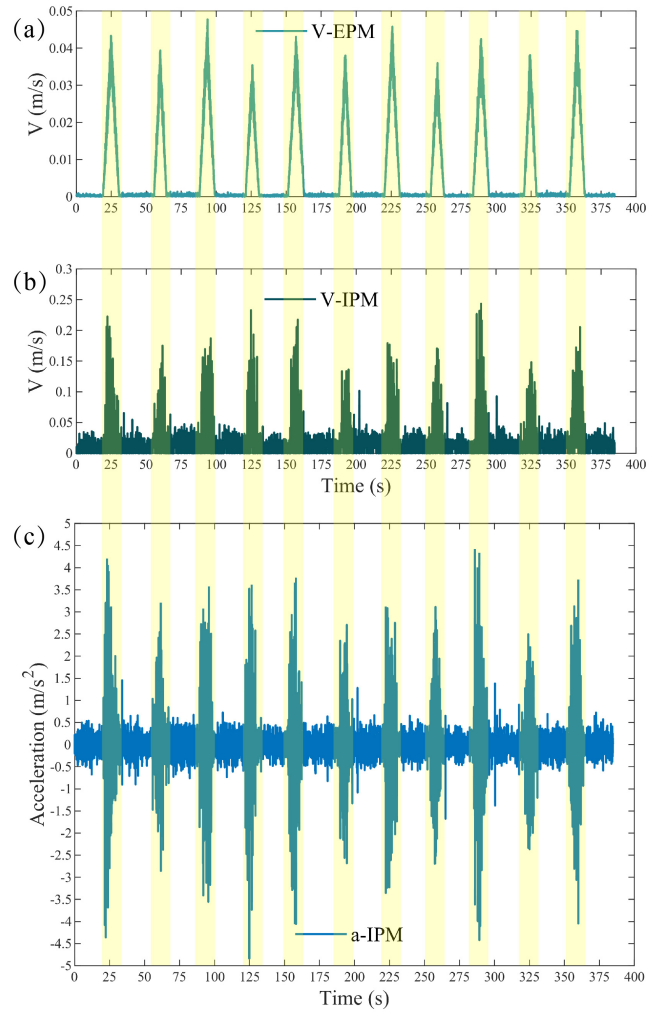


Fig. 6. (a) shows the  $\mathbf{v}$  of EPM. (d) shows the  $\mathbf{v}$  of IPM. (c) shows the  $\mathbf{a}$  of the IPM. Yellow shaded areas represent 10s line-move on the surface of PVC.

### D. Obtaining $c$ in Friction Model.

To ensure the rationality of the parameters in the given friction model, the coordinates of the end of the manipulator and the capsule robot are delivered and saved at the same frequency. The red line in Fig.7 indicates the preset trajectory of the manipulator. The IPM follows the EPM movement, which tracks point information is collected by the camera. At the same time, the coordinate information of IPM and EPM is saved in the same program based on time series. By substituting the distance of each ( $\mathbf{P}_E - \mathbf{P}_I$ ) into the Maxwell simulation [21],  $\mathbf{F}$  and  $\mathbf{F}_z$  at the corresponding time can be obtained.

In order to learn the friction model in (7), we repeat the above process to obtain more 20000 track point ( $\mathbf{P}_E$  and  $\mathbf{P}_I$ ) data (including  $\mathbf{F}$ ,  $\mathbf{F}_z$  and  $\mathbf{a}$ ). The plane test trajectory diagrams of the three mediums are as follows. All  $\mathbf{v}$ - $c$  points obtained above be plotted in the rectangular coordinate-system. We found that these scatter-charts were in line with the rule of multi-term function distribution, so



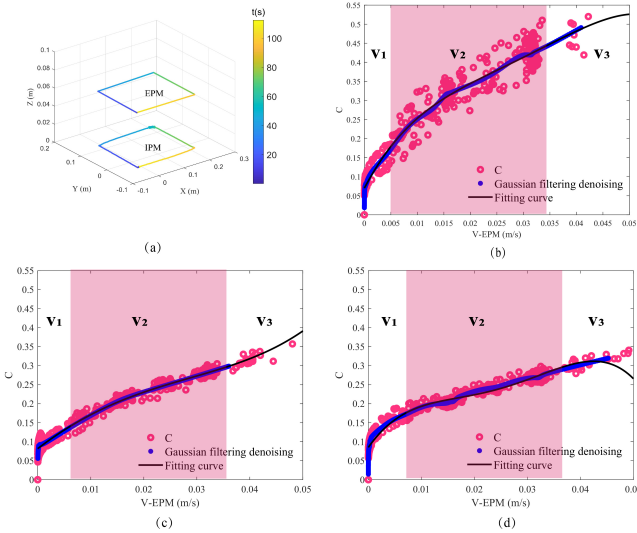


Fig. 7. (a) shows the trajectory of capsule robot and manipulator based on time series. (b), (c), (d) represents the three media movement trajectory collection points respectively, and the factor expression fitting function of the friction model obtained. The red shaded area indicates the effective speed range guided by the friction model.

polynomial curve fitting [22] be used to fit and set multi-order derivatives for the scatter-charts (as shown in Fig. 7(b)-(d)). As a result, the fifth-degree polynomial of  $v$  could fit  $c$  with small error (The sum variance between  $v$ - $c$  and the fifth-degree polynomial is 0.053 when the control speed of the manipulator is between 0.005m/s and 0.04m/s on the PVC). As same as, the three friction model formulas in different materials are obtained by matlab simulation set. The specific fitting relationship is obtained as:

$$c = p_1 * v^4 + p_2 * v^3 + p_3 * v^2 + p_4 * v + p_5 \quad (9)$$

The values of  $p_1$ ,  $p_2$ ,  $p_3$ ,  $p_4$  and  $p_5$  are listed in Table III.

TABLE III  
VALUES OF  $p_1$ ,  $p_2$ ,  $p_3$ ,  $p_4$ ,  $p_5$

Type	$p_1$	$p_2$	$p_3$	$p_4$	$p_5$
PVC	$-1.943 \times 10^5$	$2.318 \times 10^4$	-1018	26.36	0.0699
paper	$2.386 \times 10^4$	$8.069 \times 10^2$	-190.6	10.72	0.08173
polyester-cloth	$-3.75 \times 10^5$	$3.692 \times 10^4$	-1232	19.79	0.08508

## IV. EXPERIMENTAL RESULTS AND DISCUSSION

### A. Test Results of Friction model

The control experiment group is designed to test the friction model obtained in (7). The evaluation indicators of the control experimental group are trajectory following error and pressure change. Effective speed and friction factors are given in (9). Specific implementation scheme as follows: the capsule robot performs repeated motions in the same pipeline at three different speeds. Contrast tests have been carried out on smooth pipes, paper surfaces, and polyester-cloth surfaces, as shown in the actual movement scene in Fig. 8(a)-(c).

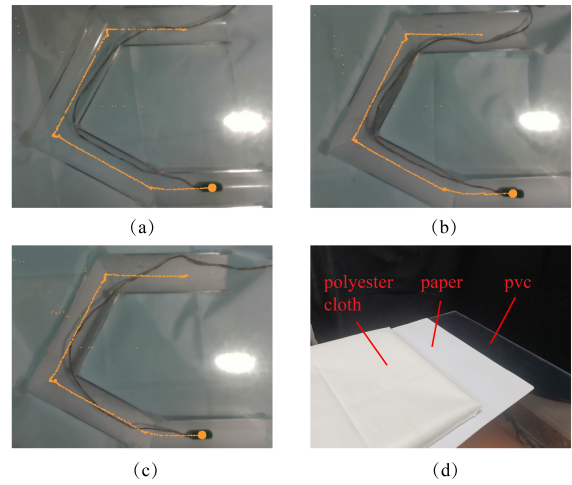


Fig. 8. The contact medium of (a) is PVC, the contact medium of (b) is paper, and the contact medium of (c) is polyester-cloth. (d) is a schematic diagram of the three materials.

TABLE IV  
AVERAGE ACCURACY (TRAJECTORY FOLLOWING ERROR) OF  $v_1$ ,  $v_2$ ,  $v_3$  UNDER THREE MEDIUMS

Error (mm)	$v_1$	$v_2$	$v_3$	Improvement
PVC	7.21	6.91	7.41	4.16% / 6.75%
paper	7.15	6.72	7.33	6.01% / 8.32%
polyester-cloth	7.05	6.63	7.17	5.95% / 7.43%

$v_1$ ,  $v_2$  and  $v_3$  represent three different velocity values on the left, middle and right of the velocity range of the friction model (as shown in Fig. 7). The values of the test speed of each medium ( $v_1$ ,  $v_2$  and  $v_3$ ), see Supplementary Video. As is shown in Fig. 8, we attach paper and cloth to the inside of the pipe to change the coefficient of friction. Table IV shows the improvement of average accuracy of  $v_2$  relative to  $v_1$  and  $v_3$  in three mediums respectively, and the values of trajectory following error on PVC are shown in Fig. 9 (b). To calculate the stability of contact force, the 1N scale-line is regarded as the standard line for the fluctuation of the contact force at the collection points in the whole trajectory. The contact force improvement of  $v_2$  is 6.12% and 6.47% compared with  $v_1$  and  $v_3$  respectively. The fluctuation of contact force on PVC is shown in Fig. 9(c). The contract force data between paper (and polyester-cloth) and the tethered capsule robot see Supplementary Video.

### B. Discussion

The friction model in this paper can be applied to improve the accuracy obviously compared the trajectory following error (7.04mm) of Zhang, P *et al.* [23]. The validity of the friction model is verified with different contact mediums shown in Fig. 8. In the futureThe contact force in current experimental scene is nearly simulation to the actual working process of the capsule. Future work as follows: First, force estimation will be added into the system to facilitate force

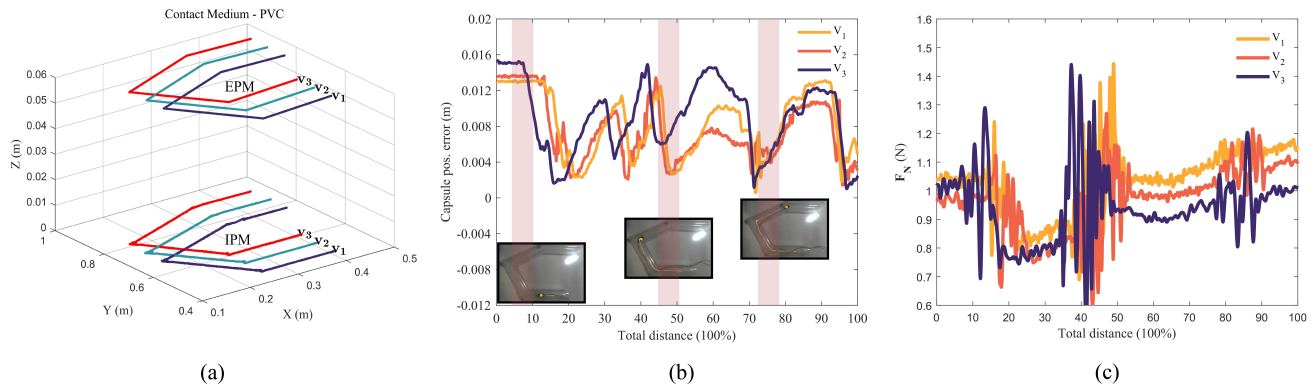


Fig. 9. The picture shows the tethered capsule robot motion on the PVC with  $v_1, v_2$ , and  $v_3$ , which are 0.045m/s, 0.02m/s, 0.005m/s respectively. (a) The trajectory graph of 10 average values of 3 sets of speed. The same color is a set of EPM and IPM trajectory control groups. (b) shows the trajectory following error at the three speeds of PVC. The three shaded areas from left to right correspond to the starting segment, the second corner, and the third corner, respectively. (c) Contact force fluctuations at three speeds.

control [24]. Second, the system will be further verified in animal experiments. Third, a more compact structure will be designed for the system.

## V. CONCLUSION

This research proposes a learning friction model for the magnet-actuated tethered capsule robot that is suitable for plane and space, and provides a method to obtain the model. The model can effectively improve the tracking accuracy and stability of the capsule movement of the preset trajectory. In addition, three mediums movement tests of friction coefficients are designed in the article. The experimental results prove that the model improves the following accuracy by about 5.6%, and the stability of the contact force is improved by about 6.2%. This experiment proves that the model is effective for the friction of any mediums tethered capsule robot. We can get the specific relationship of the tethered capsule between the control speed  $v$  and the friction factor  $c$  during the plane movement in advance, furthermore, which can be used to compensate the friction and drag force from the tethered.

## REFERENCES

- [1] P. R. Slawinski *et al.*, "Autonomously controlled magnetic flexible endoscope for colon exploration," *Gastroenterology*, vol. 154, no. 6, pp. 1577–1579, 2018.
- [2] P. Valdastri *et al.*, "Advanced technologies for gastrointestinal endoscopy," *Annual review of biomedical engineering*, vol. 14, pp. 397–429, 2012.
- [3] S. S. Mapara and V. B. Patravale, "Medical capsule robots: A renaissance for diagnostics, drug delivery and surgical treatment," *Journal of Controlled Release*, vol. 261, pp. 337–351, 2017.
- [4] L. J. Sliker *et al.*, "Frictional resistance model for tissue-capsule endoscope sliding contact in the gastrointestinal tract," *Tribology International*, vol. 102, pp. 472–484, 2016.
- [5] G. Pittiglio *et al.*, and P. Valdastri, "Magnetic levitation for soft-tethered capsule colonoscopy actuated with a single permanent magnet: A dynamic control approach," *IEEE robotics and automation letters*, vol. 4, no. 2, pp. 1224–1231, 2019.
- [6] A. W. Mahoney and J. J. Abbott, "Five-degree-of-freedom manipulation of an untethered magnetic device in fluid using a single permanent magnet with application in stomach capsule endoscopy," *The International Journal of Robotics Research*, vol. 35, no. 1-3, pp. 129–147, 2016.
- [7] M. Salehizadeh *et al.*, "Three-dimensional independent control of multiple magnetic microrobots via inter-agent forces," *The International Journal of Robotics Research*, vol. 39, no. 12, pp. 1377–1396, 2020.
- [8] G.-S. Lien *et al.*, "Magnetic control system targeted for capsule endoscopic operations in the stomach—design, fabrication, and in vitro and ex vivo evaluations," *IEEE Transactions on Biomedical Engineering*, vol. 59, no. 7, pp. 2068–2079, 2012.
- [9] C. Zhang *et al.*, "Modeling of velocity-dependent frictional resistance of a capsule robot inside an intestine," *Tribology Letters*, vol. 47, no. 2, pp. 295–301, 2012.
- [10] N. Baek, I. Sung, and D. Kim, "Frictional resistance characteristics of a capsule inside the intestine for microendoscope design," *Proceedings of the Institution of Mechanical Engineers, Part H: Journal of Engineering in Medicine*, vol. 218, no. 3, pp. 193–201, 2004.
- [11] B. Guo, Y. Liu, and S. Prasad, "Modelling of capsule–intestine contact for a self-propelled capsule robot via experimental and numerical investigation," *Nonlinear Dynamics*, vol. 98, no. 4, pp. 3155–3167, 2019.
- [12] K. Knothe, "Contact mechanics and friction: physical principles and applications," 2011.
- [13] C. Marone, "Laboratory-derived friction laws and their application to seismic faulting," *Annual Review of Earth and Planetary Sciences*, vol. 26, no. 1, pp. 643–696, 1998.
- [14] H. Allag, J.-P. Yonnet, and M. E. Latreche, "3d analytical calculation of forces between linear halbach-type permanent-magnet arrays," in *2009 8th International Symposium on Advanced Electromechanical Motion Systems & Electric Drives Joint Symposium*, pp. 1–6, IEEE, 2009.
- [15] Y. Wang *et al.*, "Learning friction model for tethered capsule robot," *arXiv preprint arXiv:2108.07151*, 2021.
- [16] M. Gao *et al.*, "Design and fabrication of a magnetic propulsion system for self-propelled capsule endoscope," *IEEE Transactions on Biomedical Engineering*, vol. 57, no. 12, pp. 2891–2902, 2010.
- [17] K. Giannoukos and K. Salonitis, "Study of the mechanism of friction on functionally active tribological polyvinyl chloride (pvc)–aggregate composite surfaces," *Tribology International*, vol. 141, p. 105906, 2020.
- [18] S. Zhihani Hervan *et al.*, "Hardness, friction and wear characteristics of 3d-printed pla polymer," *Proceedings of the Institution of Mechanical Engineers, Part J: Journal of Engineering Tribology*, vol. 235, no. 8, pp. 1590–1598, 2021.
- [19] A. Johansson *et al.*, "Paper friction—influence of measurement conditions," *Tappi journal*, vol. 81, no. 5, pp. 175–184, 1998.
- [20] M. Robins *et al.*, "The friction of polyester textile fibres," *Journal of Physics D: Applied Physics*, vol. 17, no. 7, p. 1349, 1984.
- [21] J. Ku *et al.*, "Accurate calculation of major forces acting on magnetic particles in a high-gradient magnetic field: A 3d finite element analysis," *Powder Technology*, 2021.
- [22] V. MATLAB, "9.3. 0.713579 (r2017b)," *The Math-Works Inc., Natick, MA*, 2017.
- [23] P. Zhang *et al.*, "Endoluminal motion recognition of a magnetically-

guided capsule endoscope based on capsule-tissue interaction force,” *Sensors*, vol. 21, no. 7, p. 2395, 2021.

[24] X. Gao *et al.*, “Learning force-relevant skills from human demonstration,” *Complexity*, vol. 2019, 2019.